J Mater Sci (2018) 53:7735–7743

Energy materials

A dyeing-induced heteroatom-co-doped route toward flexible carbon electrode derived from silk fabric

Xin Li[1], Jing Zhao[1], Zaisheng Cai[1], and Fengyan Ge[1,*]

[1] *Key Lab of Science and Technology of Eco-textile, Ministry of Education College of Chemistry, Chemical Engineering and Biotechnology, Donghua University, Shanghai 201620, China*

Received: 23 December 2017
Accepted: 31 January 2018
Published online: 20 February 2018

ABSTRACT

Flexible carbon electrode with high performance from silk fabric was fabricated by a simple approach. Silk fabric was uniformly dyed with heteroatom-enriched dye molecules by a traditional dyeing process, followed by direct pyrolysis. The as-prepared heteroatom-co-doped carbonized silk fabric exhibits a significantly improved electrochemical performance with the specific capacitance of 255.95 F g^{-1} at the scan rate of 2 mV s^{-1} using 1 M Na_2SO_4 electrolyte, a wide operation voltage window as well as a good cycling life stability (8% capacitance loss over 5000 cycles). The excellent capacitive performance can be attributed to the multiple synergistic effects between the double-layer capacitance (hierarchical porosity, good wettability and conductivity) and the extra pseudocapacitance (N, O and S heteroatom co-doping). Moreover, the carbonized dyed silk fabric possesses wearability and lightweight. Importantly, the convenient approach can provide industrial-grade production of heteroatom-co-doped silk fabric-based carbon electrode materials for applications in flexible energy storage devices.

Introduction

During the past few years, the fast development of wearable electronics has dramatically promoted the needs for flexible energy storage devices [1–3]. Flexible supercapacitors have been regarded as one of the most promising energy storage devices due to their high power density, fast charge–discharge rate and long cycle life [4, 5]. As an indispensable functional block of supercapacitors, flexible electrodes with high efficiency have attracted more attention. Recently, various types of flexible materials, including papers [6, 7], polymeric films [8, 9], fibers/yarns [10, 11] and fabrics [12–16], have been served as electrode materials for supercapacitors. Among them, commercial fabrics represent an interesting option to prepare flexible electrodes, owing to their inherent softness, excellent mechanical strength, high porosity and the capability to be integrated into clothes for directly wearable devices [17]. Generally, the fabrics do not possess good electric conductivity. It is of significant importance for the fabric-based electrode to own a high conductivity. Directly carbonizing is a simple

Address correspondence to E-mail: DHUfyge@163.com

https://doi.org/10.1007/s10853-018-2100-3

approach to convert the commercial fabrics into carbonized fabrics with good electrical conductivity. Bao et al. [12] fabricated highly conductive and flexible activated carbon textiles by directly carbonizing cotton T-shirt for the application of energy storage. He et al. [13] carbonized natural flax fabrics as raw materials in preparing flexible and binder-free electrode materials for supercapacitors. However, the capacitances of the above-mentioned directly carbonized fabrics were relatively low, and other materials such as metal oxides and electrically conducting polymers were used to further improve the electrochemical performance of fabric-based supercapacitors [14, 15].

Heteroatom functionalities to carbon electrode materials are of great importance to induce their electron–donor properties and control the electrochemical performances of their surfaces [18, 19]. The introduction of heteroatoms can not only provide extra pseudocapacitance through the faradaic redox reaction between electrolyte ions and carbon surface [20], but also improve the surface wettability of electrode in aqueous electrolyte through enhancing numbers of hydrophilic polar sites on the electrode surface [18]. Recently, it is reported that heteroatoms such as N, S, P and B can be incorporated into carbon material to improve their performance. Compared with single heteroatom doping, co-doping can produce the synergetic effect, leading to further improvement in the overall performance [21].

The dyeing procedures with large-scale production have been widely applied in the textile industry for thousands of years. The aim of dyeing is to add color throughout the fabrics by dipping the fabrics in the dye bath. In the dyeing process, various kinds of dyes are utilized and these dye molecules containing enriched O, N and S heteroatoms can uniformly penetrate into the hierarchical fabrics skeleton. By directly carbonizing the dyed fabrics, the carbonized fabric-based electrodes with heteroatom co-doping can be obtained. Therefore, the dyeing method can simply realize multi-heteroatoms doping.

Silk is a kind of widely used natural biomaterials. It is composed of fibroin and sericin, which contain about 98% of protein [22]. The high content of protein in silk fiber provides enriched nitrogen and oxygen functionalities, which may facilitate the increase in pseudocapacitance. Commercially available silk fabrics (SF) exhibit hierarchical structures with interlacing warp and weft yarns in the vertical and horizontal directions. These unique structures provide possibility to achieve good stretchability and 3D framework, resulting in superior interconnected performance as a flexible electrode. Furthermore, silk fabrics can be directly transformed into conductive graphitic structures through a simple heating treatment. Ma et al. [23] fabricated a transparent all-solid supercapacitors by carbonizing a pristine silk fabric, but the specific capacitance of the carbonized silk fabric (CSF) is relatively low (940 μF cm^{-2} at a scan rate of 5 mV s^{-1}). The extra pseudocapacitive materials were further added to enhance the whole capacitance. According to the above-mentioned analysis, it can be speculated that heteroatom co-doping will effectively improve the capacitive performance of the carbonized silk fabrics. However, to the best of our knowledge, the manufacture of heteroatom-co-doped carbonized silk fabrics for flexible electrode materials has not been explored.

In this study, we report a novel route to fabricate a flexible carbon electrode material. The commercial silk fabric was dyed with an acid dye and followed by direct carbonization. The obtained carbon electrode exhibits good wettability, wearability, lightweight and excellent electrochemical performance. More importantly, the simple approach facilitates a low-cost and scale-up production of flexible electrode materials as promising candidates to wearable energy devices.

Experimental

Synthesis of flexible carbonized fabric electrode

The commercial silk fabric (69 g m^{-2}, Wensli Group Co., Ltd, China) was washed with ethanol and deionized water and then dried at room temperature. A piece of 1-g pretreated silk fabric (SF) was dyed at the dye concentration 10% o.w.f (percentage on weigh of dye to fabric, % o.w.f) at a liquor ratio of 100:1, with the dye bath being maintained at pH < 7 by the addition of 0.2 g L^{-1} acetic acid. The dyeing process is carried out according to Fig. S1. Firstly, 0.1 g Red 3B acid dye (Shanghai Anoky Group Co., Ltd.) and 1 g SF were added into 100 mL deionized water and stirred for 5 min. 0.01 g L^{-1} dispersant IW (Jiangsu Haian Petrochemical plant, China) and 0.1 g Na_2SO_4 were introduced to the bath. Secondly, the

temperature was raised to 95 °C at a heating rate of 1.5 °C min^{-1} and maintained at this level for 45 min. Finally, the temperature was dropped to room temperature and silk fabric dyed with red dye (SF-R) was thoroughly washed with cold water, squeezed and dried. SF was directly carbonized in nitrogen at 900 °C for 2 h at a heating rate of 2 °C min^{-1} and cooled to room temperature at 5 °C min^{-1}. The carbonized silk fabric is denoted as CSF. The dyed silk fabric (SF-R) carbonized with the same procedure is named as CSF-R, in which *R* represents red acid dye.

Characterization

Morphology of the samples was imaged by using a scanning electron microscope (SEM, HITACHI/TM-1000, Japan), and Raman spectrometer (inVia-Reflex, UK). X-ray photoelectron spectroscopy (XPS, Thermo 250XL, USA) was applied to characterize the element speciation analysis. The surface contact angels (CA) of the obtained materials were measured by a goniometer (Kruss DSA 30, German). The specific surface area and pore volume were analyzed using nitrogen adsorption–desorption isotherms that were obtained using a surface area and a porosimetry analyzer (TriStarII3020 M) at − 196 °C. The pore sizes and distributions of macro-pores in fabrics were measured using a bubble-point method on a capillary flow porometer (CFP, 1100 A, USA).

Electrochemical characterization

All electrochemical characterizations were measured on a CHI 660 Eelectrochemical workstation (Shanghai Chenhua Instruments Co.) at room temperature. For the three-electrode system, carbon materials with an active area (1 cm^2) were used as the working electrode. Pt foil and Ag/AgCl electrode were used as the counter and reference electrodes, respectively. The electrochemical performance was tested in 1 M Na_2SO_4 electrolyte. The specific capacitance was calculated from the cyclic voltammetry (CV) curves according to the following equation:

$$C = \frac{1}{v \cdot m \cdot \Delta V} \int_{V0}^{V0+\Delta V} i dV$$

where v (mV s^{-1}) is the scan rate, m (g) is the mass of the working electrode, ΔV (V) is the working potential window. The galvanostatic charge–discharge (GCD) tests were carried out at the range of current density from 2 to 10 mA cm^{-2}. The electrochemical impedance spectroscopy (EIS) was recorded in the frequency range of 0.01 Hz–100 kHz with a potential amplitude of 5 mV.

Results and discussion

Silk is a kind of natural protein fiber consisting of a series of amino acid with functional groups of amino and carboxyl [24]. As a common type of dye, acid dye is widely used for dyeing of wool and silk in an acidic bath. The mechanism of silk fabric dyed with acid dye is shown in Scheme 1. Under acidic conditions, ionic bonds ($–SO_3^-$ NH_3^+) between the protonated amino groups of fibers and sulfonate ions of acid dyes will be formed. Furthermore, there are other strong interactions between fibers and dyes also including hydrogen bonds and Van der Waals forces. When the dye reacted with the fibers, this indicated abundant N, O and a little S heteroatoms originating from Red 3B acid dye were introduced into the silk fabrics. In Scheme 1, the uniformity and penetrability of the dyed silk were observed by a light microscope. From cross-sectional photograph of dyed fibers, it was clearly found that the inner parts of fibers were fully colored, which meant the dye molecules penetrated well in the fibers to realize deep dye. The longitudinal section image of dyed fibers also displayed that dye molecules were uniformly deposited on the fibers. Therefore, the effective N, O and S co-doping to silk fabric could be realized by the traditional dyeing technique.

SEM was carried out to investigate surface morphological changes of the silk fabrics at micro-nanoscale during the dyeing and carbonizing procedure (Fig. 1). Originally, the SF exhibited smooth surface with interlacing warp and weft yarns in the vertical and horizontal directions (Fig. 1a). As shown in Fig. 1b, after dyeing, there was no any change in the morphology for SF-R. Notably, after pyrolysis, SF-R lost ~ 84% in weight, the fibers of CSF-R shrank from ~ 12 to ~ 6.5 μm in diameter (Fig. 1c). Despite the shrinkage, CSF-R still maintained originally well-formed 3D-woven structures. The 3D texture structure of CSF-R could avoid over-loading and offer rapid ion transport with an improved rate capability.

CSF and CSF-R were characterized by Raman spectra, as shown in Fig. 2a. The peak located at 1338 cm^{-1} (D-band) was attributed to the disordered

Scheme 1 The formation mechanism of heteroatom-co-doped CSF-R.

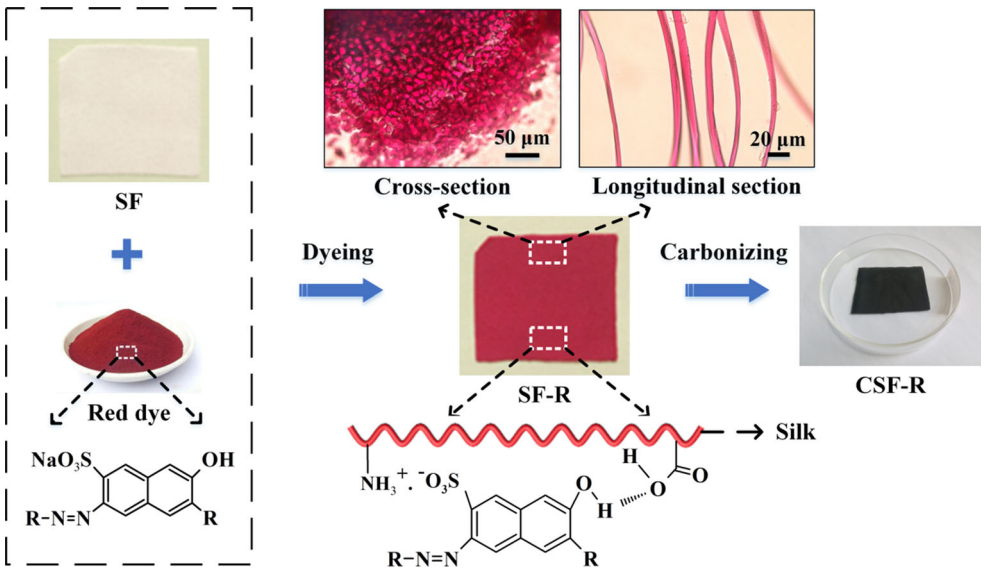

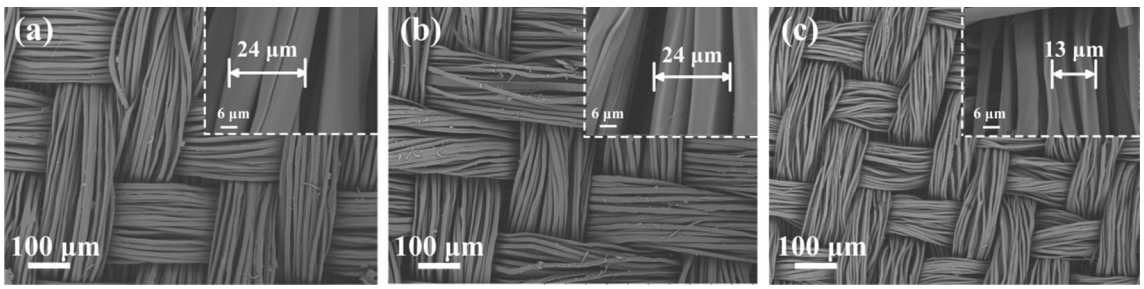

Figure 1 SEM images of **a** SF, **b** SF-R and **c** CSF-R.

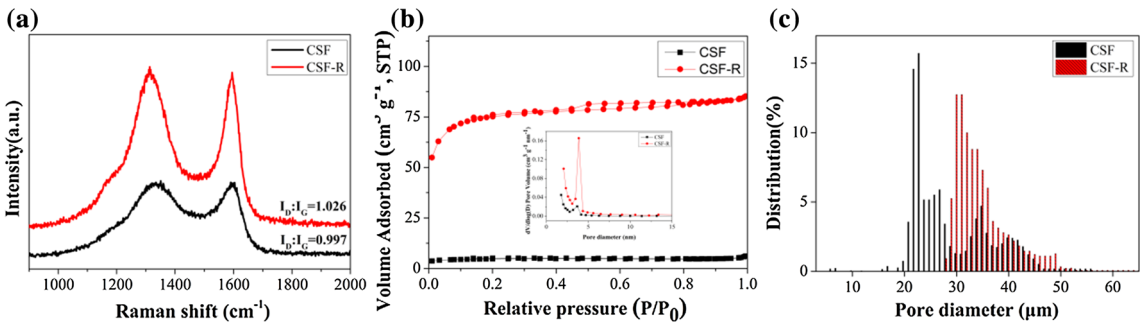

Figure 2 **a** Raman spectra, **b** N_2 adsorption–desorption isotherms and pore size distributions (inset) and **c** evolutions of pore size distributions for CSF and CSF-R.

carbon or defective graphite, and other one at 1580 cm^{-1} (G-bond) was assigned to the stretching bond of sp^2-hybridized carbon [25]. The D/G ratio of band intensities indicated the degree of structural disorder with respect to a defective graphitic structure. It was calculated that the integrated intensity ratio (I_D/I_G) of CSF-R (1.026) was higher than that of CSF (0.997). The increase of I_D/I_G could be attributed to the defective structure induced by heteroatom doping from dye molecules.

The porosities of CSF and CSF-R were investigated using N_2 adsorption–desorption isotherms. As displayed in Fig. 2b, CSF generated type I adsorption–desorption isotherm, indicating a typical microporous structure. CSF-R showed type I + IV isotherm with steep uptake at a low relative pressure (0–0.2) and noticeable hysteresis loop at higher relative

pressure (0.4–1.0), suggesting the coexistence of both micropore and meso-pore structures in this material. Furthermore, the specific surface area of CSF-R was determined to be 256.6 $m^2\ g^{-1}$ (as seen in Table S1 of supporting information), which was higher than that of CSF (16.3 $m^2\ g^{-1}$), demonstrating the surface area of CSF-R had a great increase via dyeing treatment. The corresponding pore size distributions (PSD) are displayed in the inset of Fig. 2b. The pores size for CSF was centered at 1.76 nm, which represented micropores. Compared with CSF, CSF-R owned larger meso-pore structure with 3.87 nm diameter. The formation of meso-pores from CSF-R might be ascribed to the evaporation and decomposition of less stable dye molecules inside the silk fabric during the thermal treatment. The pore size evolutions were further performed to study the distributions of macro-pores for CSF and CSF-R. As shown in Fig. 2c, distributions of the peaks for CSF and CSF-R were centered at 23 and 31 μm, respectively. It indicated that CSF-R had bigger pores than CSF in the range of large pore size (> 50 nm). CSF-R possessed a hierarchical porous structure including micro-, meso- and macro-pores. The micropores can play a crucial role for developing the electrical double-layer surfaces to reach high capacitance, while meso-pores and macro-pores can provide not only good charge propagation during high current loads with low resistance, but also wide transport paths for ion diffusion into micropores to enhance the capacitor performance [26–28]. In general, such hierarchical porosity of CSF-R is beneficial for enhancement of performance for electrode materials.

XPS was performed to further ascertain the chemical state of the heteroatoms in CSF and CSF-R. As shown in Fig. 3a, the fully scanned spectra of CSF and CSF-R showed the presence of C, O and N as the main components of the materials. Meanwhile, elemental mapping images in Fig. S2 also further proved that heteroatoms, N, O, were uniformly incorporated into carbon framework. In addition, compared with CSF, S heteroatom could be observed from the fully scanned spectrum of CSF-R. The relative contents of each element on surface of these samples are summarized in Table 1. In comparison with CSF, N, O and S contents of CSF-R exhibited a sharp increase. The reason could be attributed to the dyeing process, in which N, O and S heteroatoms were introduced into the carbon framework.

The high-resolution C 1*s* spectra are given in Fig. S3, and the main peak at 283.6 eV assigned to sp^2-hybridized carbon indicated that most of carbon atoms were aromatic carbon in the samples. As shown in Fig. 3c and f, the N 1*s* spectra of the CSF and CSF-R consisted of four components including pyridinic-N at 397.3 eV, pyrrolic-N at 399.3 eV, graphitic-N at 400.3 eV and oxidized-N at 402.1 eV. Generally, it was suggested that the presence of graphitic-N and oxidized-N might facilitate the electron transfer in the carbon skeleton to enhance the electronic conductivity of carbon materials [29]. The pyridine-N and pyrrolic-N at the edges of the carbon framework usually induced more disorders and provided extra pseudocapacitance [30]. Compared to CSF (73.3%), CSF-R exhibited higher pyridinic-N and pyrrolic-N contents (88.4%), implying lower graphitic structure. The result fitted well with the Raman spectra. As revealed in Fig. 3d, g, the deconvoluted O 1*s* spectra for CSF and CSF-R consisted of three similar peaks. Compared to CSF, the relative content of these peaks in O=C–OH/C–OH and C–O–C/SO_X for CSF-R had a significant increase, which attributed to hydroxyl and sulfonic acid groups of dye molecules introduced by the dyeing treatment. As shown in Fig. 3e, h, the distinct peaks almost at 163.2 eV emerged in the *S* spectra of CSF and CSF-R, corresponding to thiophene-S (C-S-C). The other peaks at 167.8 and 169.8 eV were assigned to oxidized sulfur (C-SO_x-C). Compared with CSF, the binding energies of oxidized sulfur for CSF-R exhibited sharp increase. The reason might be explained on the introduction of sulfonic acid groups from the dye molecules. The observation was also confirmed by above-mentioned O 1*s* spectra analysis. The doped-S is beneficial for tuning the electronic properties of graphene, polarizing electron pairs easily and creating charge sites [31]. In general, XPS analysis illustrated these heteroatoms were successfully introduced to carbon skeleton by the dyeing technique. As literatures reported, heteroatom doping could not only provide extra pseudocapacitance through the faradaic redox reaction [20], but also improve the surface wettability of electrode. The water contact angles of CSF and CSF-R were measured and the results are listed in Fig. 3b. Compared with CSF, CSF-R displayed a great decrease in the contact angle as low as 79°, indicating a better wettability. This reason was attributed to the increase in hydrophilic polar sites on the electrode

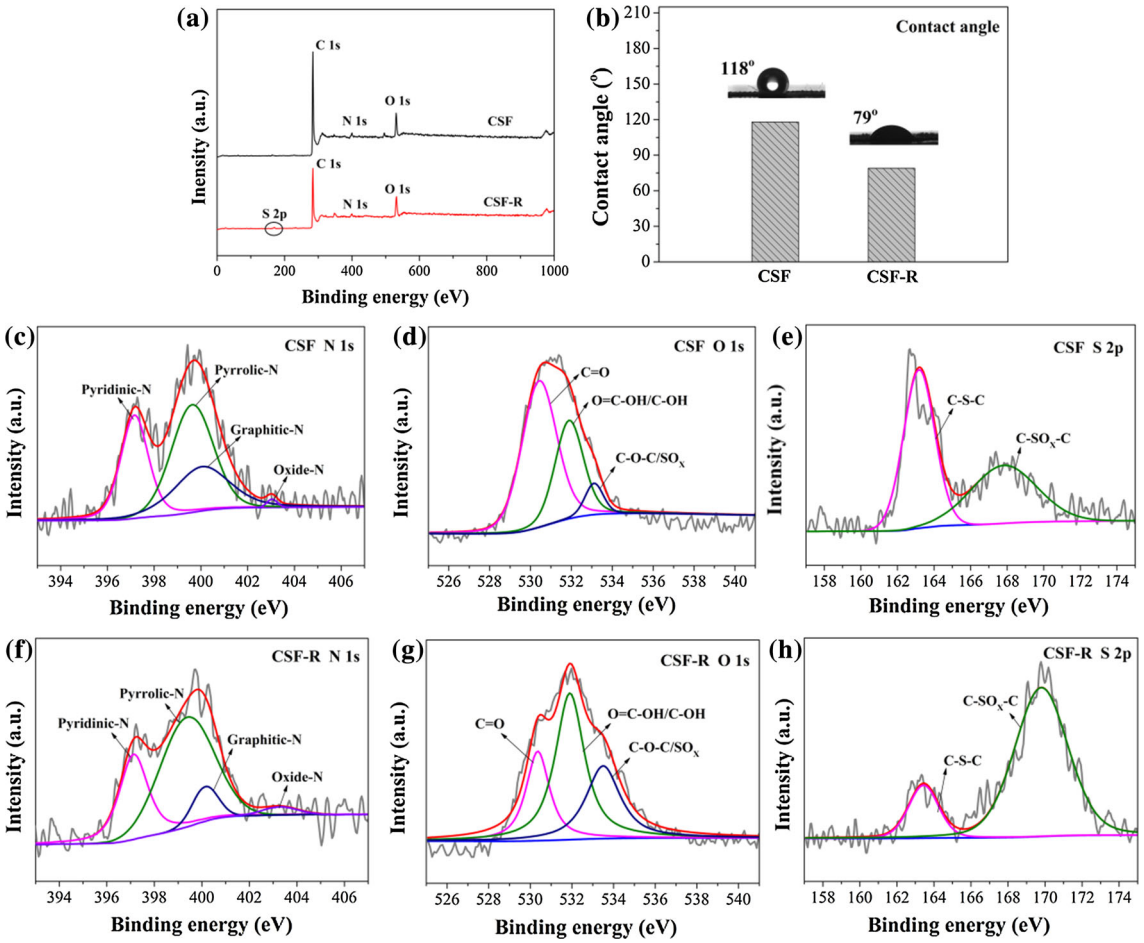

Figure 3 XPS spectra of **a** full survey scan; **c**–**e** N 1*s*, O 1*s*, S 2*p* of CSF; **f**–**h** N 1*s*, O 1*s*, S 2*p* of CSF-R; **b** water contact angles of CSF and CSF-R.

Table 1 Elemental composition obtained from XPS analysis of all samples

Sample	Atomic composition (%)				
	C	N	O	S	N+O+S
CSF	85.60	3.84	9.87	0.69	14.40
CSF-R	79.99	4.35	14.44	1.22	20.01

surface by dyeing-induced heteroatom co-doping [18].

To estimate the electrochemical performance of CSF-R, CV and GCD were investigated in a three-electrode system using 1 M Na_2SO_4 aqueous electrolyte at room temperature. As seen in Fig. 4a, CV curves presented a nearly ideal rectangular shape without significant distortion even with the scan rate increased from 2 to 100 mV s^{-1}, manifesting the ideal capacitive behavior of carbon electrode. Calculated from the CV curves, the specific capacitance of CSF-R reached 255.95 F g^{-1} at a scan rate of 2 mV s^{-1}. As shown in Fig. 4b, when the scan rate increased from 2 to 20 mV s^{-1}, about 45% of its initial value was retained, showing a good rate capability of CSF-R electrode. In accordance with the CV results, CSF-R depicted a long charge–discharge time, as displayed in Fig. 4c. The charge time was equivalent to the discharge time, proving excellent coulombic efficiency.

To investigate the effects on the electrochemical performances of a dyeing-induced heteroatom co-doping, CV curves of CSF and CSF-R were measured at a scan rate of 2 mV s^{-1}. As displayed in Fig. 4d, the CV curve area of CSF was negligible, suggesting the small specific capacitance. CSF-R exhibited a high specific capacitance of 255.95 F g^{-1}, which was more than five times higher than that of CSF (45.69 F g^{-1}).

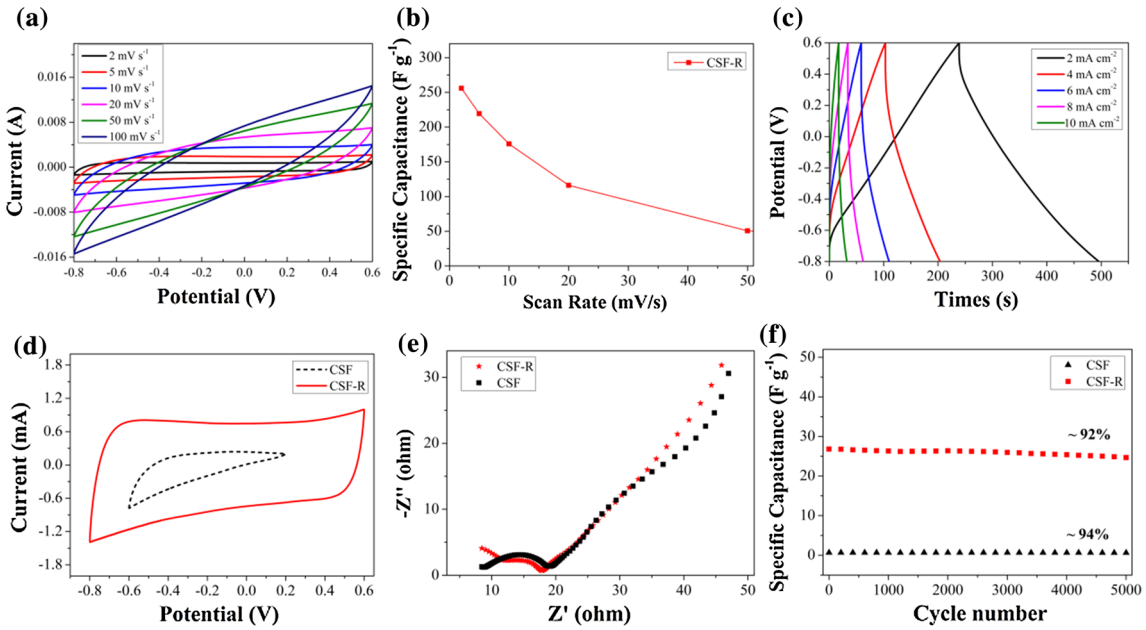

Figure 4 **a** CV curves at different scan rates from 2 to 100 mV s^{-1} in a voltage window from − 0.8 to 0.6 V of CSF-R, **b** specific capacitance of CSF-R at different scan rates, **c** GCD curves at different current densities from 2 to 10 mA cm^{-2} of CSF-R, **d** CV curves at 2 mV s^{-1} of all samples, **e** comparative Nyquist plots of all samples under the influence of an amplitude of 5 mV and **f** cycling stability of all samples at the scan rate of 100 mV s^{-1} to 5000 cycles.

These indicated the better capacitive behavior of CSF-R. Moreover, compared with CSF, CSF-R expressed a wide operation voltage window in the range from − 0.8 to 0.6 V. The wide voltage window of CSF-R originated from more heteroatom functionalities, unique hierarchical porous-woven structure and the application of neutral electrolyte [29]. Next, electrochemical impedance spectroscopy (EIS) of CSF and CSF-R was further recorded with a frequency range from 0.01 Hz to 100 kHz, as shown in Fig. 4e. It was well accepted that the equivalent series resistance (ESR) of the samples was associated with the diameter of the semicircle in the intermediate frequency region of Nyquist plots [32]. Compared to CSF, CSF-R exhibited smaller semicircles, indicating an improved electrical conductivity. The result was in agreement with the square resistance measurements (as seen in Fig. S4). The reason could be due to electron donor/acceptor properties of heteroatom functionalities, which were introduced by dyeing process. As shown in Fig. 4f, the capacitance stability of CSF-R was remarkably high, with still 92% maintained ratio after 5000 charge–discharge cycles, suggesting the excellent long-term cyclic stability and a potential application as an electrode for supercapacitors.

In general, the above results demonstrate that CSF-R possesses a large and stable energy storage performance. The improved electrochemical performances can be attributed to the multiple synergistic effects as following: (1) The excellent double-layer capacitance originates from interconnected texture frameworks with hierarchical porous structure including macro-pores, meso-pores and micropores. (2) The good wettability can be attributed to numbers of hydrophilic polar sites incorporated by heteroatoms, which can improve the overall capacitance. (3) The good conductivity is due to electron donor/acceptor properties of heteroatom co-doping. (4) The extra pseudocapacitance generated by N, O and S heteroatom co-doping can be ascribed to the dye molecules. The above four elements have favorable multiple synergistic effects to improve CSF-R electrode material performance for flexible energy storage applications.

In addition, the obtained carbon fabric-based electrode displayed its potential application in wearable electronics, which had been characterized by lightweight and potentially foldable properties (as shown in Fig. S5).

Conclusion

In summary, we employed a dyeing followed by direct carbonization process to convert commercial silk fabrics into heteroatom-co-doped interconnected carbon electrodes. As proved by experiment, N, O and S heteroatom functionalities were uniformly incorporated into the 3D texture structure to facilitate the enhancement of pseudocapacitance and wettability. The co-doped carbonized silk fabric demonstrates superior electrochemical performance with the specific capacitance of 255.95 F g^{-1} at the scan rate of 2 mV s^{-1}, a wide operation voltage window as well as good cycling life stability (92% capacitance retention after 5000 cycles). The excellent capacitive performance can be attributed to the multiple synergistic effects between the double-layer capacitance (hierarchical porosity, good wettability and electric conductivity) and the extra pseudocapacitance (N, O and S heteroatoms originating from the dye molecules). Importantly, the simple approach facilitates a novel route for low-cost and easy scale-up production of flexible silk fabric-based electrode materials as promising candidates to wearable energy devices.

Acknowledgements

This work was supported by the National Natural Science Foundation of China (No. 51203018).

Electronic supplementary material: The online version of this article (https://doi.org/10.1007/s10853-018-2100-3) contains supplementary material, which is available to authorized users.

References

[1] Wei C, Xu Q, Chen Z, Rao W, Fan L, Yuan Y, Bai Z, Xu J (2017) An all-solid-state yarn supercapacitor using cotton yarn electrodes coated with polypyrrole nanotubes. Carbohydr Polym 169:50–57

[2] Ye X, Zhou Q, Jia C, Tang Z, Wan Z, Wu X (2016) A knittable fibriform supercapacitor based on natural cotton thread coated with graphene and carbon nanoparticles. Electrochim Acta 206:155–164

[3] Zhao J, Li X, Cai ZS, Ge FY (2017) A flexible carbon electrode based on traditional cotton woven fabrics with excellent capacitance. J Mater Sci 52(3):1–7. https://doi.org/10.1007/s10853-017-1161-z

[4] Zhang H, Yan Q, Lu Z (2016) Fully-printed ultra-flexible supercapacitor supported by a single-textile substrate. ACS Appl Mater Interfaces 8(47):32317–32323

[5] Chen J, Wei H, Fu N, Chen H, Lan G, Lin H, Han S (2018) Facile synthesis of nitrogen-containing porous carbon as electrode materials for superior-performance electrical double-layer capacitors. J Mater Sci 53(3):2137–2148. https://doi.org/10.1007/s10853-017-1664-7

[6] Feng J-X, Li Q, Lu X-F, Tong Y-X, Li G-R (2014) Flexible symmetrical planar supercapacitors based on multi-layered MnO_2/Ni/graphite/paper electrodes with high-efficient electrochemical energy storage. J Mater Chem A 2(9):2985–2992

[7] Singu DC, Joseph B, Velmurugan V, Ravuri S, Grace AN (2017) Combustion synthesis of graphene from waste paper for high performance supercapacitor electrodes. Int J Nanosci 17:1760023

[8] Suganya N, Jaisankar V, Sivakumar EKT (2017) Conducting polymeric hydrogel electrolyte based on carboxymethylcellulose and polyacrylamide/polyaniline for supercapacitor applications. Int J Nanosci 17:1760003

[9] Shi S, Xu C, Yang C, Chen Y, Liu J, Kang F (2013) Flexible asymmetric supercapacitors based on ultrathin two-dimensional nanosheets with outstanding electrochemical performance and aesthetic property. Sci Rep 3(6150):2598

[10] Huang Y, Peng L, Liu Y, Zhao G, Chen JY, Yu G (2016) Biobased nano porous active carbon fibers for high-performance supercapacitors. ACS Appl Mater Interfaces 8(24):15205–15215

[11] Choi C, Lee JM, Kim SH, Kim SJ, Di J, Baughman RH (2016) Twistable and stretchable sandwich structured fiber for wearable sensors and supercapacitors. Nano Lett 16(12):7677–7684

[12] Bao L, Li X (2012) Towards textile energy storage from cotton T-shirts. Advanced materials 24(24):3246–3252

[13] He S, Chen W (2015) Application of biomass-derived flexible carbon cloth coated with MnO_2 nanosheets in supercapacitors. J Power Sour 294:150–158

[14] Liang Y, Wu D, Fu R (2013) Carbon microfibers with hierarchical porous structure from electrospun fiber-like natural biopolymer. Sci Rep 3(7):1119

[15] Xue J, Zhao Y, Cheng H, Hu C, Hu Y, Meng Y, Shao H, Zhang Z, Qu L (2013) An all-cotton-derived, arbitrarily foldable, high-rate, electrochemical supercapacitor. Phys Chem Chem Phys 15(21):8042–8045

[16] Zhu Yh, Yuan S, Bao D, Yb Yin, Hx Zhong, Xb Zhang, Jm Yan, Jiang Q (2017) Decorating waste cloth via industrial

wastewater for tube-type flexible and wearable sodium-ion batteries. Adv Mater 29:1603719

[17] Jost K, Stenger D, Perez CR, McDonough JK, Lian K, Gogotsi Y, Dion G (2013) Knitted and screen printed carbon-fiber supercapacitors for applications in wearable electronics. Energy Environ Sci 6(9):2698–2705

[18] Zhou DD, Li WY, Dong XL, Wang YG, Wang CX, Xia YY (2013) A nitrogen-doped ordered mesoporous carbon nanofiber array for supercapacitors. J Mater Chem A 1(29):8488–8496

[19] Chen LF, Zhang XD, Liang HW, Kong M, Guan QF, Chen P, Wu ZY, Yu SH (2012) Synthesis of nitrogen-doped porous carbon nanofibers as an efficient electrode material for supercapacitors. ACS Nano 6(8):7092–7102

[20] Razmjooei F, Singh K, Kang TH, Chaudhari N, Yuan J, Yu JS (2017) Urine to highly porous heteroatom-doped carbons for supercapacitor: a value added journey for human waste. Sci Rep 7(1):10910

[21] Tang C, Liu Y, Yang D, Yang M, Li H (2017) Oxygen and nitrogen co-doped porous carbons with finely-layered schistose structure for high-rate-performance supercapacitors. Carbon 122:538–546

[22] Uddin K, Hossain S (2010) A comparitive study on silk dyeing with acid dye and reactive dye. Int J Eng Technol 10(6):21–26

[23] Ma D, Ma Y, Chen Z, Hu A (2017) A silk fabric derived carbon fibre net for transparent capacitive touch pads and all-solid supercapacitors. J Mater Chem A 5(39):20608–20614

[24] Wang C, Li X, Gao E, Jian M, Xia K, Wang Q, Xu Z, Ren T, Zhang Y (2016) Wearable strain sensors: carbonized silk fabric for ultrastretchable, highly sensitive, and wearable strain sensors (Adv. Mater. 31/2016). Adv Mater 28(31):6640–6648

[25] Genovese M, Jiang J, Lian K, Holm N (2015) High capacitive performance of exfoliated biochar nanosheets from biomass waste corn cob. J Mater Chem A 3(6):2903–2913

[26] Hou J, Cao C, Idrees F, Ma X (2015) Hierarchical porous nitrogen-doped carbon nanosheets derived from silk for ultrahigh-capacity battery anodes and supercapacitors. ACS Nano 9(3):2556–2564

[27] Alabadi A, Yang X, Dong Z, Li Z, Tan B (2014) Nitrogen-doped activated carbons derived from a co-polymer for high supercapacitor performance. J Mater Chem A 2(30):11697–11705

[28] Xia K, Gao Q, Jiang J, Hu J (2008) Hierarchical porous carbons with controlled micropores and mesopores for supercapacitor electrode materials. Carbon 46(13):1718–1726

[29] Li X, Wang J, Zhao Y, Ge F, Komarneni S, Cai Z (2016) Wearable solid-state supercapacitors operating at high working voltage with a flexible nanocomposite electrode. ACS Appl Mater Interfaces 8(39):25905–25914

[30] Liu R, Pan L, Wan L, Wu D (2015) An evaporation-induced tri-consistent assembly route towards nitrogen-doped carbon microfibers with ordered mesopores for high performance supercapacitors. Phys Chem Chem Phys 17(6):4724–4729

[31] Kotal M, Kim J, Kim KJ, Oh IK (2016) Sulfur and nitrogen co-doped graphene electrodes for high-performance ionic artificial muscles. Adv Mater 28(8):1610–1615

[32] Xie Q, Bao R, Xie C, Zheng A, Wu S, Zhang Y, Zhang R, Zhao P (2016) Core-shell N-doped active carbon fiber@graphene composites for aqueous symmetric supercapacitors with high-energy and high-power density. J Power Sources 317:133–142